Synthesis, Structure, and Magnetic Properties of Co, Ni, and Co−Ni Alloy Nanocluster-Doped SiO_2 Films by Sol−Gel Processing

G. Mattei,* C. de Julián Fernández, P. Mazzoldi, and C. Sada

INFM, Dipartimento di Fisica, Università di Padova, via Marzolo 8, I-35131 Padova, Italy

G. De

Sol−Gel Division, Central Glass and Ceramic Research Institute, 196 Raja S.C. Mullick Road, Kolkata 700032, India

G. Battaglin

INFM, Dipartimento di Chimica Fisica, Università di Venezia, Calle Larga S. Marta 2137, I-30123 Padova, Italy

C. Sangregorio and D. Gatteschi

Dipartimento di Chimica, Università di Firenze, via della Lastruccia 5, I-50019 Sesto Fiorentino (Firenze), Italy

Received January 11, 2002. Revised Manuscript Received May 22, 2002

The optical, structural, and magnetic properties of Co, Ni, and Co_xNi_{100-x} ($0 < x < 100$) alloy nanoclusters in silica host obtained by the sol−gel route are presented. Throughout the entire range of composition investigated, from pure Ni to pure Co, the nanoclusters exhibit an fcc structure, with lattice parameters increasing with the Co fraction in the system. This indicates Co−Ni alloy formation. It has also been observed that the average cluster diameter increases with increasing Co fraction in the system. An enhancement of the magnetic moment was exhibited in the pure Co and Ni samples, and good agreement between the measured values and those of the corresponding bulk alloys was found for the other samples. All composites are superparamagnetic at room temperature.

1. Introduction

The study of the physical and chemical properties of nanoparticulated composites has received much interest because of their new physical properties and their potential applications.[1] In particular, it has been observed that magnetic particles with sizes in the nanometer range exhibit features that are quite different from those of the corresponding bulk magnets, including modifications of the intrinsic properties,[2,3] superparamagnetism,[3−5] enhanced coercitivity,[3] shifts of the hysteresis loops,[6,7] or the absence of magnetic saturation at high fields.[7] Also, nanoparticles embedded in dielectric matrixes present enhanced magnetoresistance[8,9] and good magnetooptical features.[10] This departure from bulklike behavior might be due to several reasons: modifications of the electronic structure,[11] the interplay between surface and volume properties,[3] chemical interactions between the nanocluster and the embedding matrix,[12,13] or interparticle interactions.[5] As a consequence, magnetic nanoclusters have been gaining importance in recent days because of their possible applications in magnetic recording media[3] and catalysis.[14] Moreover, alloy-based nanocomposites can add a further degree of freedom, i.e., the composition, which is expected to play a crucial role in tailoring new magnetic

* Corresponding author. Fax: +39.049.8277003. Phone: +39.049.8277045. E-mail: mattei@padova.infm.it.

(1) Singh Nalwa, H., Ed. *Handbook of Nanostructured Materials and Nanotechnology*; Academic Press: San Diego, 2000.

(2) Himpsel, F. J.; Ortega, J. E.; Mankey, G. J.; Willis, R. F. *Adv. Phys.* **1998**, *47* (4), 511−597.

(3) Chien, C. L. *Science and Technology of Nanostructures Magnetic Materials*; Hadjipanayis, G., Prinz, G. A., Eds.; Plenum Press: New York, 1991; Vol. 259, pp 477−495.

(4) Bean, C. P.; Livingstoon, J. D. *J. Appl. Phys.* **1959**, *30*, 120S.

(5) Dormann, J. L.; Fiorani, D.; Tronc, E. *Adv. Chem. Phys.* **1997**, *98*, 283−494.

(6) Gangopadhyay, S.; Hadjipanayis, G.; Sorensen, C. M.; Klabunde, K. J. *Nanostructured Materials*; Pergamon Press: Oxford, U.K., 1992; Vol. 1, pp 449−456.

(7) Respaud, M.; Broto, J. M.; Rakoto, H.; Fert, A. R.; Thomas, L.; Barbara, B.; Verelst, M.; Snoeck, E.; Lecante, P.; Mosset, A.; Osuna, J.; Ould Ely, T.; Amiens, C.; Chaudret, B. *Phys. Rev. B* **1998**, *57* (5), 2925−2935.

(8) Xu, Q. Y.; Chen, H.; Sang, H.; Yin, X. B.; Ni, G.; Lu, J.; Wang, M.; Du, Y. W. *J. Magn. Magn. Mater.* **1999**, *204*, 73−78.

(9) Yakushiji, K.; Mitani, S.; Takanashi, K.; Ha, J.-G.; Fujimori, H. *J. Magn. Magn. Mater.* **2000**, *212*, 75−81.

(10) Kraus, G. T.; Lu, Y.-C.; Trancik, J. E.; Mitro, D. M.; Giannelis, E. P.; Thompson, M. O.; Sass, S. L. *J. Appl. Phys.* **1997**, *82* (3), 1189−1195.

(11) Billas, I. M. L.; Chatelain, A.; de Heer, W. A. *J. Magn. Magn. Mater.* **1997**, *168*, 64−84.

(12) Kodama, R. H.; Edelstein, A. S. *J. Appl. Phys.* **1999**, *85* (5), 4316−4318.

(13) Smith, J. A.; Limthongkul, P.; Hartsuyker, L.; Kim, S. Y.; Sass, S. L. *J. Appl. Phys.* **1998**, *83* (5), 2719−2726.

(14) Tihay, F.; Pourroy, G. R.-P. M.; Roger, A. C.; Kiennemann, A. *Applied Catalysis A* **2000**, *206*, 24−42.

10.1021/cm021106r CCC: $22.00
Published on Web 07/12/2002

Table 1. Sol−Gel-Synthesized Co−Ni Nanocluster-Doped SiO_2 Films: Measured Film Thickness *t*

sample	*t* (nm)	$C_{Co}/C_{Ni}/C_{Si}$[a] (nominal)	$(C_{Co}+C_{Ni})^b/C_{Si}$ (RBS ± 5%)
Co_{100}	148 ± 3[c]	10:0:90	9.5:90.5
$Co_{80}Ni_{20}$	134 ± 3[c]	8:2:90	10.5:89.5
$Co_{75}Ni_{25}$	135 ± 3[c]	7.5:2.5:90	10:90
$Co_{70}Ni_{30}$	148 ± 3[c]	7:3:90	10:90
$Co_{66}Ni_{33}$	160 ± 3[c]	6.6:3.3:90	9.9:90.1
$Co_{50}Ni_{50}$	150 ± 15[d]	5:5:90	10.5:89.5
$Co_{33}Ni_{66}$	140 ± 14[d]	3.3:6.6:90	9.6:90.4
Ni_{100}	148 ± 3[c]	0:10:90	10:90

[a] Nominal molar concentrations *C* of Co, Ni, and Si. [b] RBS measured Co plus Ni molar concentration (the associated error is about 5%). [c] Measured by TEM. [d] Measured by RBS.

properties in such systems.[15] Therefore, careful control of these parameters is of paramount importance in the synthesis of new alloy-based materials. This control can be made difficult by the different chemical reactivities of two metals with the matrix, which can promote separation (via oxidation, for instance) instead of alloying of the species.

The sol−gel technique is able to control both cluster[16] and matrix[17] composition. From the point of view of magnetic applications, this technique has been used to synthesize alloy nanoclusters involving mainly transition metals, e.g., Nd−Fe,[18] Fe−Cr,[19] Fe−Ni,[20] Cu−Ni,[21] and Fe−Co.[22] In this paper, we report the sol−gel preparation and systematic structural and compositional analysis of a series of nanoclusters consisting of the ferromagnetic 3d elements Co and Ni and their intermediate alloys embedded in a silica host. The general molar composition of the nanoclusters is Co_xNi_{100-x} with $x = 100$, 80, 75, 70, 66, 50, 33, and 0 to cover the entire phase diagram of the Co−Ni system from pure Co ($x = 100$) to pure Ni ($x = 0$). The Co−Ni bulk alloy phase diagram presents, for Co compositions larger than 70%, a structural transition from fcc to hcp that modifies all of the physical properties of the system.[23] Indeed, Co−Ni alloys within this range of composition present higher values of coercivity and remanence and are used for magnetic recording media.[24]

2. Experimental Section

Film compositions (in moles) are given in Table 1. The pure Co, pure Ni, and Co−Ni codoped silica films were prepared by the sol−gel dip-coating technique. The sols were prepared starting from $Si(OC_2H_5)_4$ (TEOS), $Co(NO_3)_3{\cdot}6H_2O$, $Ni(NO_3)_3{\cdot}6H_2O$, catalytic amount of HNO_3, H_2O, *n*-propanol, and isobutanol. The film composition [i.e., the molar ratio of total metal (pure or mixed Co + Ni) to SiO_2] was kept constant in all of the films at 10 equiv mol % metal/90% SiO_2 (see Table 1). The general preparation method of these films is as follows: The required amount of TEOS was first dissolved in *n*-propanol (50% of the total amount). To this mixture, the required amount of metal salt solution (dissolved in water and then acidified with HNO_3) was added with stirring. A residual amount of *n*-propanol (50%) was then added, and the solution was stirred for 30 min. After this period, isobutanol was added, and the sol was stirred for another hour. The total H_2O/TEOS and HNO_3/TEOS molar ratios were 6 and 0.01, respectively. The water of crystallization of the metal salts was also taken into account. The total equivalent oxide (including dopants) content of the sols was about 5.5 wt % in all cases. Thoroughly cleaned silica glasses (type II, Heraeus) were used as substrates. For the dip-coating preparation, a withdrawal velocity of 10−12 cm/min was maintained. The resulting films were dried at 60 °C. Then, the samples were first heated to 500 °C in air (the heating rate was about 200 °C/h) to remove the organic matter and to obtain pure and/or mixed cobalt−nickel oxide-doped silica films. The temperature was then raised from 500 to 800 °C (the heating rate was 150 °C/h) in an 8% H_2−92% N_2 gas atmosphere (in the following, indicated simply as H_2-N_2) and held for 1 h. After the holding time, the furnace was allowed to cool naturally to 450 °C (about 70 min) while the H_2-N_2 atmosphere was maintained. Then, the samples were pushed to a cooler part of the furnace (about 300 °C) and kept there for 15 min, after which they were further pushed to a 40 °C region and kept there for 15 min. All operations were done in H_2-N_2 atmosphere. These final (i.e., after H_2-N_2 annealing) samples are labeled Co_xNi_{100-x}, where $x = 100$, 80, 75, 70, 66, 50, 33, and 0, and have a general film composition of 10 mol % metal−90% silica.

The cobalt−nickel, silicon, and oxygen contents in the films were determined by Rutherford backscattering spectrometry (RBS). A $^4He^+$ beam at an energy of 2.2 MeV was used. Optical absorption spectra were measured in the wavelength region from 200 to 800 nm by using a Cary UV−vis−NIR dual-beam spectrophotometer. Samples for transmission electron microscopy (TEM) were prepared in planar and cross-sectional views as reported in ref 16 and examined at the CNR-LAMEL Institute in Bologna, Italy, with a Philips CM30-T TEM instrument operating at 300 kV equipped with an EDAX energy-dispersive X-ray spectrometer (EDS) for compositional analysis. The magnetic characterization was carried out using a Cryogenic S600 SQUID magnetometer with the magnetic field applied in the plane of the silica slides and the magnetic moment measured in that direction.

3. Results and Discussion

Silica films containing pure Co and Ni and six intermediate Co−Ni alloys were prepared and their compositions were checked by Rutherford backscattering (RBS) technique. As the atomic weights of Co and Ni are similar, these metals cannot be differentiated by RBS; therefore, only the total concentration of Co and Ni was obtained by this technique. The results, reported in Table 1, were in good agreement with the nominal compositions of the film samples.

3.1. Optical Absorption. After the air annealing at 500 °C for 30 min to remove the organic material, the sol−gel films were faintly bluish in color and showed characteristic absorption bands of Ni^{2+} and Co^{2+} ions having T_d symmetry in an amorphous silica host as has also been observed by other workers.[25−27] These 500 °C air-baked films were further heated in H_2-N_2 atmosphere to 800 °C to reduce the metal ions. The evolution of the optical spectrum of the sample $Co_{50}Ni_{50}$ (after H_2-N_2 annealing for 1 h) is presented in Figure 1.

(15) Chen, C.; Kitakami, O.; Okatomo, S.; Shimada, Y. *J. Appl. Phys.* **1999**, *86* (4), 2161−2165.
(16) De, G.; Mattei, G.; Mazzoldi, P.; Sada, C.; Battaglin, G.; Quaranta, A. *Chem. Mater.* **2000**, *12* (8), 2157−2160.
(17) Gonella, F.; Mazzoldi, P. *Handbook of Nanostructured Materials and Nanotechnology*; Singh Nalwa, H., Ed.; Academic Press: San Diego, 2000; Vol. 4.
(18) Li, J.; Liu, S.; Qian, X.; Bayi, J.; Su, M. *J. Alloys Compd.* **1996**, *238*, 113−115.
(19) Chatterjee, A.; Das, D.; Chakravorty, D.; Choudhury, K. *Appl. Phys. Lett.* **1990**, *57* (13), 1360−1362.
(20) Wang, J.-P.; Han, D.-H.; Luo, H.-L.; Gao, N.-F.; Liu, Y.-Y. *J. Magn. Magn. Mater.* **1994**, *135*, L251.
(21) Kaiser, A.; Gorsmann, C.; Schubert, U. *J. Sol−Gel Sci. Technol.* **1997**, *8*795−799.
(22) Hou, D. L.; Tang, G. D.; Chen, W.; Liu, Y.; Nie, X. F.; Luo, H.-L. *Phys. Status Solidi A* **1998**, *169*, 131−137.
(23) *Ferromagnetism*; Bozorth, R. M., Ed.; Van Nostrand Company: New York, 1951.
(24) Bate, G.; Altsted, J. H. *IEEE Trans. Magn.* **1969**, *MAG-5*, 821.

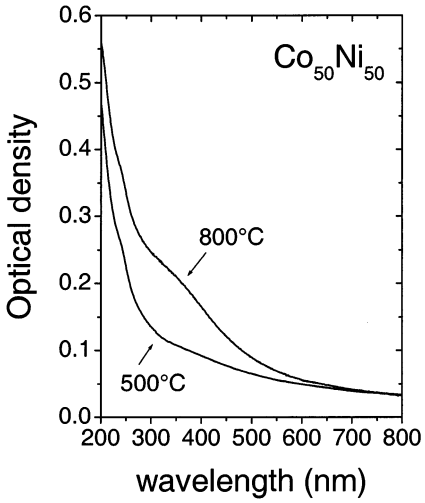

Figure 1. Evolution of the optical absorption spectrum of the sample $Co_{50}Ni_{50}$ after air annealing for 30 min at 500 °C and after a subsequent annealing in H_2-N_2 for 1 h at 800 °C.

The optical spectra of pure Ni and Co nanocluster-doped films obtained after annealing at 800 °C in H_2-N_2 atmosphere are displayed in Figure 2a and are similar to the theoretical spectra simulated considering 5-nm-diameter clusters embedded in SiO_2 ($n = 1.46$) using Mie theory[28] (see Figure 2b). As can be seen, the surface plasmon resonance (which is very sharp in noble metals[28]) is almost completely damped by the interband transitions involving partially filled d bands. Therefore, the optical spectra exhibit only a very broad band centered near 340 nm and a shoulder near 300 nm for Ni- and Co-cluster doped SiO_2, respectively. This is a qualitative indication that metallic reduction took place in both cases. The optical spectra of the samples containing either Co or Ni are presented in Figure 2c and exhibit absorption bands that are intermediate between those of pure Ni and Co systems. However, because of the small differences in the optical spectra as a function of composition, it is not possible to make quantitative conclusions on the actual cluster composition.

3.2. TEM. A systematic structural and compositional investigation was carried out on the samples by TEM. The bright-field cross-sectional micrographs of Co−Ni samples are shown in Figure 3. In all of the cases investigated, well-defined spherical particles with dimensions in the nanometer range can be observed on the amorphous background of the matrix in a layer of about 120−150 nm thickness from the surface. The sample Ni_{100} exhibits some small voids inside the film (Figure 3a), suggesting that incomplete densification of the matrix occurred during annealing. This phenomenon is absent in all of the other samples. The film thickness measured by TEM is reported in Table 1, except for the samples $Co_{33}Ni_{66}$ and $Co_{50}Ni_{50}$, examined as planar sections, for which the values obtained by RBS are reported. Figure 4 shows the histograms of the diameter distribution for all of the samples as obtained by TEM

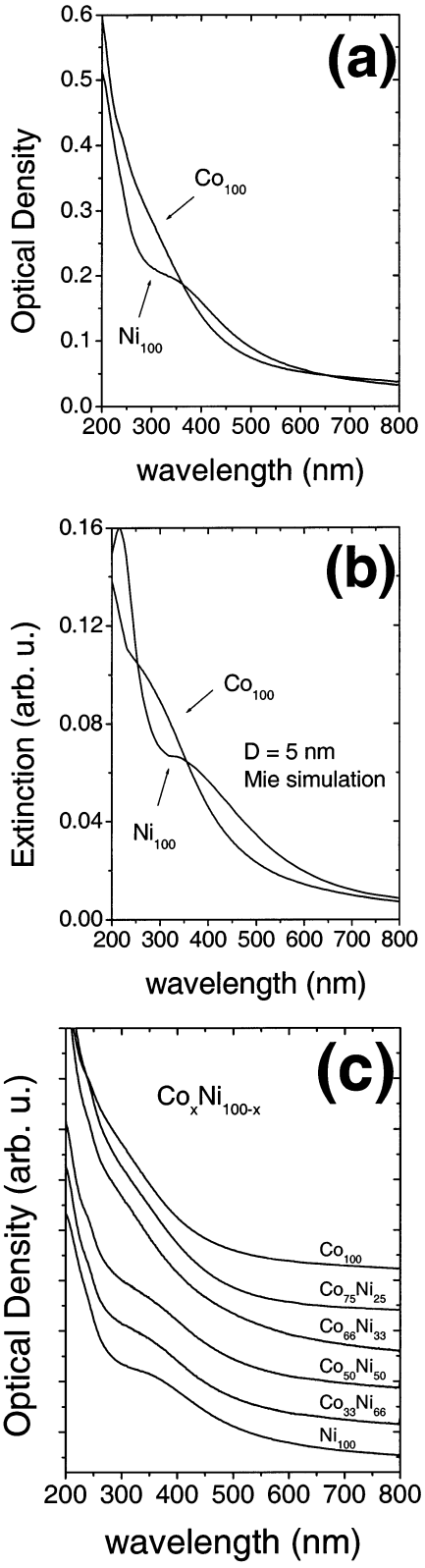

Figure 2. (a) Optical absorption spectra of the samples Co_{100} and Ni_{100} after annealing in H_2-N_2 for 1 h at 800 °C. (b) Mie simulation of the extinction cross section of 5-nm-diameter Co or Ni clusters in SiO_2 (refractive index $n = 1.46$). (c) Optical absorption spectra of the samples Co_xNi_{100-x} with $x = 100$, 75, 66, 50, 33, and 0. The spectra are vertically shifted for better clarity.

analysis: nonlinear fits to this distribution with log−normal and Gaussian functions results in slightly lower χ^2 values for the Gaussian distribution. A monotonic

(25) Orgaz, F.; Rawson, H. *J. Non-Cryst. Solids* **1986**, *82*, 378.
(26) Duran, A.; Fernandez Navaro, J. M.; Mazon, P.; Joglar, A. *J. Non-Cryst. Solids* **1988**, *100*, 494.
(27) Roy, S.; Ganguli, D. *J. Non-Cryst. Solids* **1992**, *151*, 203.
(28) Kreibig, U.; Vollmer, M. *Optical Properties of Metal Clusters*; Springer-Verlag: Berlin, 1995.

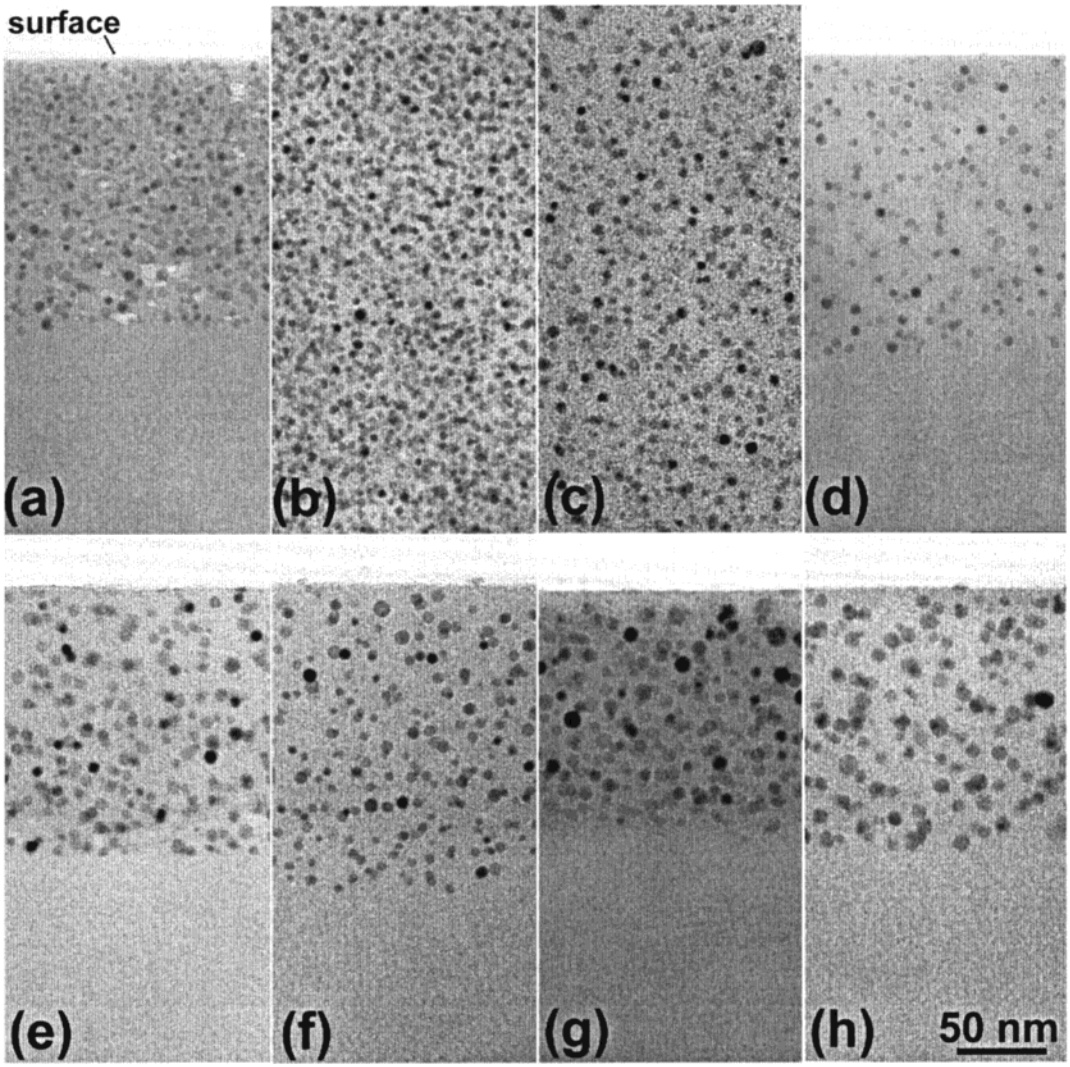

Figure 3. Cross-sectional TEM bright-field images of the samples Co_xNi_{100-x}: (a) $x = 0$ (pure Ni), (b) $x = 33$ (planar view), (c) $x = 50$ (planar view), (d) $x = 66$, (e) $x = 70$, (f) $x = 75$, (g) $x = 80$, (h) $x = 100$ (pure Co).

evolution of the average particle size from $\langle D \rangle = 3.1 \pm 1.1$ nm (average value ± standard deviation of the experimental distribution) to $\langle D \rangle = 6.5 \pm 1.1$ nm was observed with increasing Co fraction in the system, as reported in Figure 5 (the error bar at each experimental point is the standard deviation).

We also analyzed the samples with selected area electron diffraction (SAED) to investigate the crystalline structure of the clusters. For all of the analyzed compositions, the SAED pattern exhibits Debye−Scherrer rings of a single fcc phase, as shown in Figure 6a for the $Co_{70}Ni_{30}$ sample. Considering that the bulk Co−Ni alloy presents (according to the bulk phase diagram) a single hcp alloy phase when the Co fraction is greater than 75%,[29] this result is clear evidence of the stabilization of an otherwise metastable phase occurring either as a size effect or as a result of an increased interaction between the particle surface and the matrix. The fact that this stabilization of the fcc phase is not simply triggered by the Ni content can be further understood by considering that the Co_{100} sample also exhibits a single fcc phase. Indeed, the bulk stable Co structure at room temperature is hcp ($P6_3/mmc$, with $a = 0.2505$ nm and $c = 0.4060$ nm), which transforms via a martensitic transition into a Co fcc phase ($Fm3m$, $a = 0.354\,47$ nm) that is stable above 450 °C.

Bulk nickel has an fcc structure ($Fm3m$, $a = 0.352\,38$ nm), and its lattice parameter differs from that of the bulk Co fcc phase by 0.0021 nm, which is at the limit of SAED quantification technique. Therefore, to better calibrate the SAED pattern, an internal Si standard was used (a piece of monocrystalline Si was glued in front of the sample during TEM sample preparation). The SAED spectra were radially averaged,[30] and from the resulting intensity profiles (presented in Figure 6b), the lattice parameter was extracted. The results of the SAED analysis are summarized in Table 2 for all of the compositions investigated. Just for comparison, Table 2 also reports the fcc lattice parameters of a theoretical Vegard Co−Ni alloy calculated at the Co fractions corresponding to the Co/Ni molar ratios measured by EDS at the Co K and Ni K shells (last column of Table 2). Even if the error bars in the SAED quantification are not much smaller than the difference between lattice

(29) *Magnetic Properties of Metals*; Wijn, H. P. J., Ed.; Data in Science and Technology; Springer Verlag: Berlin, 1991.

(30) Hammersley, A. P.; Svensson, S. O.; Hanfland, M.; Fitch, A. N.; HΣusermann, D. *High Pressure Res.* **1996**, *14*, 235.

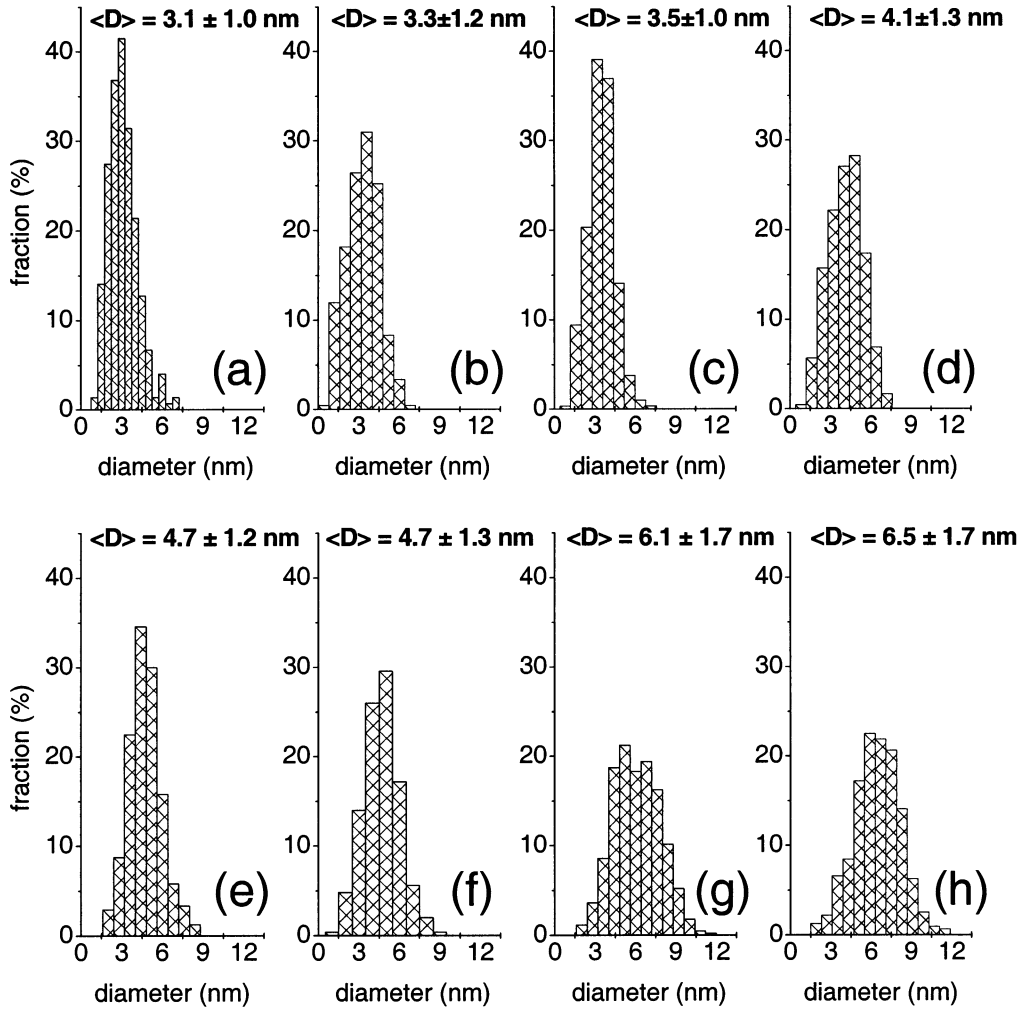

Figure 4. Size distribution histograms from a TEM analysis of the samples Co_xNi_{100-x}: (a) $x = 0$ (pure Ni), (b) $x = 33$, (c) $x = 50$, (d) $x = 66$, (e) $x = 70$, (f) $x = 75$, (g) $x = 80$, (h) $x = 100$ (pure Co).

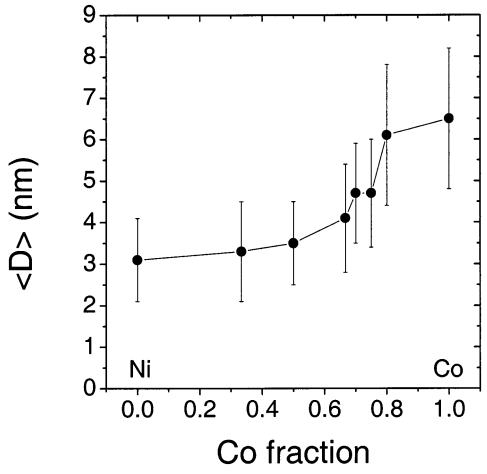

Figure 5. Evolution of the average diameter as a function of the Co fraction in the system deduced from the TEM size distribution in the samples Co_xNi_{100-x}.

parameters of bulk fcc Co and fcc Ni structures, Figure 7 shows an increase in the SAED measured lattice constant as a function of Co fraction in the system, indicating Co−Ni fcc alloy formation. No evidence of crystalline cobalt−nickel oxides or silicates (which would give reflections at $1/d$ values lower than those actually observed) can be extracted from the SAED analysis (see, for instance, the SAED pattern in Figure 6a). Up to now, it has not been clear why the Co−Ni system also stabilizes in our samples in the fcc phase when the Co molar fraction in the system is near 1. It is interesting to mention that Co−Ni alloy clusters with similar or smaller sizes, embedded in silica, have been synthesized by our group[31] by sequential ion implantation of Co and Ni at different doses without post-implantation annealing. In that case, above Co fractions of about 0.7, the coexistence of fcc and hcp phases was evidenced by SAED analysis. This is an indication that size is not the main factor triggering the final structure of the clusters. We stress the fact that, during sol−gel synthesis, both the matrix and the Co_xNi_{100-x} clusters are formed at high temperature (800 °C), where the fcc phase is the stable phase for the bulk. It is well-known that the martensitic transformation from fcc to hcp bulk Co generally ends with coexistence of the two phases and that it is not suppressed by fast cooling rates.[32] Therefore, a possible explanation of our results could be the fact that, during the cooling process (which lasts for about 2 h and, therefore does not quench the system),

(31) de Julián Fernández, C.; Sangregorio, C.; Mattei, G.; Maurizio, C.; Battaglin, G.; Gonella, F.; Lascialfari, A.; Lo Russo, S.; Gatteschi, D.; Mazzoldi, P.; González, J. M.; D'Acapito, F. *Nucl. Instrum. Meth. Phys. Res. B* **2001**, *175−177*, 468−473.

(32) Christian, J. W. *Proc. R. Soc. London* **1951**, *206*, 51−64.

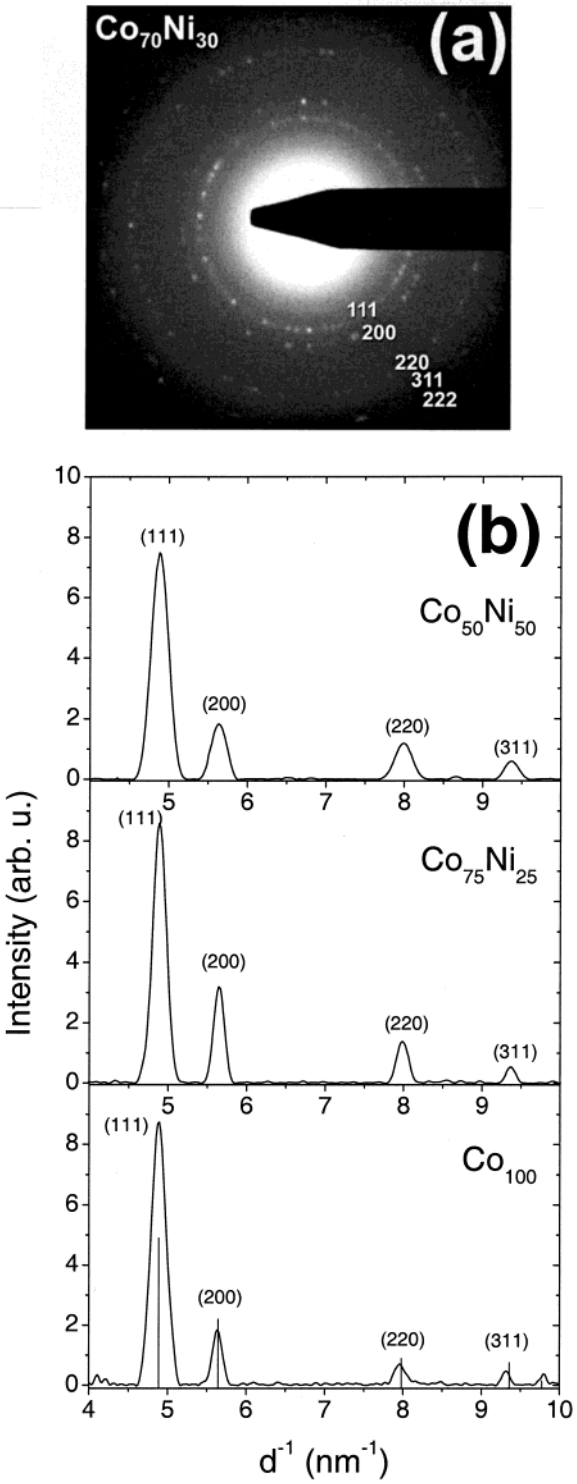

Figure 6. (a) SAED pattern of $Co_{70}Ni_{30}$ after annealing in H_2-N_2 for 1 h at 800 °C. (b) Radially averaged SAED profiles of some Co_xNi_{100-x} samples after annealing in H_2-N_2 for 1 h at 800 °C: (upper panel) $x = 50$, (middle panel) $x = 75$, (lower panel) $x = 100$ (pure Co). Vertical lines indicate the reflections for bulk fcc Co.

there is no strong driving force that constrains the clusters to change their phase, allowing the system to relax into the fcc state, whose stabilization at room temperature can be further assisted by the nanometric dimensions of the particles.[33]

(33) Sato, H.; Kitakami, O.; Sakurai, T.; Shimada, Y.; Otani, Y.; Fukamichi *J. Appl. Phys.* **1996**, *81* (4), 1858−1862.

Table 2. TEM−SAED Results on Co−Ni Nanocluster-Doped SiO_2 Films

sample	cluster diameter[a] (nm)	a_{fcc}[b] (nm) (SAED)	a_{fcc}[c] (nm) (Vegard's law)	C_{Co}/C_{Ni}[d] (nominal)	C_{Co}/C_{Ni}[e] (EDS)
Co_{100}	6.5 ± 1.7	0.3545(12)	0.354 47	–	–
$Co_{80}Ni_{20}$	6.1 ± 1.7	0.3539(12)	0.354 05	4.0	3.6 ± 0.2
$Co_{75}Ni_{25}$	4.7 ± 1.3	0.3540(12)	0.353 95	3.0	2.9 ± 0.2
$Co_{70}Ni_{30}$	4.7 ± 1.2	0.3536(12)	0.353 84	2.33	2.2 ± 0.2
$Co_{66}Ni_{33}$	4.1 ± 1.3	0.3538(15)	0.353 77	2.0	1.9 ± 0.1
$Co_{50}Ni_{50}$	3.5 ± 1.0	0.3532(15)	0.353 42	1.0	1.0 ± 0.1
$Co_{33}Ni_{66}$	3.3 ± 1.2	0.3528(18)	0.353 08	0.5	0.51 ± 0.04
Ni_{100}	3.1 ± 1.0	0.3519(12)	0.352 38	0	0

[a] Average value ± standard deviation. [b] fcc lattice parameter from SAED analysis. [c] fcc lattice parameter from Vegard's law assuming the Co/Ni molar ratio measured by EDS. [d] Nominal Co/Ni molar ratio. [e] Co/Ni molar ratio measured by EDS.

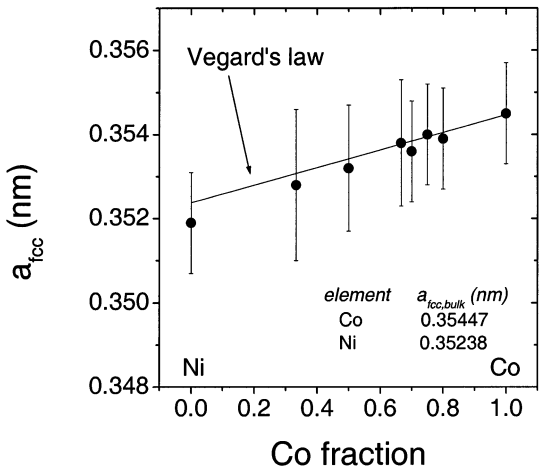

Figure 7. Evolution of the fcc lattice parameter (filled circles) as a function of the Co fraction in the system obtained from SAED analysis of the samples Co_xNi_{100-x}. For comparison, the solid line represents the calculated Vegard lattice parameters of a Co−Ni fcc alloy.

3.3. Magnetic Properties. The formation of the alloy in these materials has been further studied through an analysis of the magnetic moment per atom as a function of the Co/Ni ratio. In bulk Co−Ni alloys, the magnetic moment per atom varies almost linearly between the Ni and the fcc Co values, which are 0.6 μ_B and 1.80 μ_B,[23] respectively. For each sample, the magnetic field dependence of the magnetization was measured at 3 K up to a maximum applied field of 6 T. The magnetic contributions of the sample holder and of the silica slide were separately measured and subtracted from the measured data. The magnetic moment per atom was calculated (with an accuracy of about 10%) considering all Co and Ni atoms, whose concentration was obtained from RBS measurements. The corrected magnetization curves are shown in Figure 8. For all samples, a technical saturation was reached above about 2 T. In Figure 9, the magnetic moment per atom at 6 T is reported for all of the samples (circles), together with the corresponding values for the bulk alloys (dashed line). A good agreement between the magnetic moment values of the present Co−Ni samples and the corresponding bulk samples is observed, except for the values of the pure Ni and pure Co samples, which are larger. A reason that might explain the observed enhancement is that the annealing (and reduction) at 800 °C is not able to fully eliminate free ions trapped in the matrix.

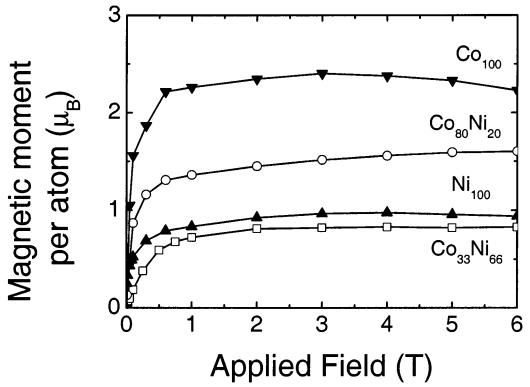

Figure 8. Variation of the magnetic moment per atom as a function of the applied field at 3 K for the Co_{100} (down triangles), $Co_{80}Ni_{20}$ (circles), $Co_{33}Ni_{66}$ (squares), and Ni_{100} (up triangles) samples.

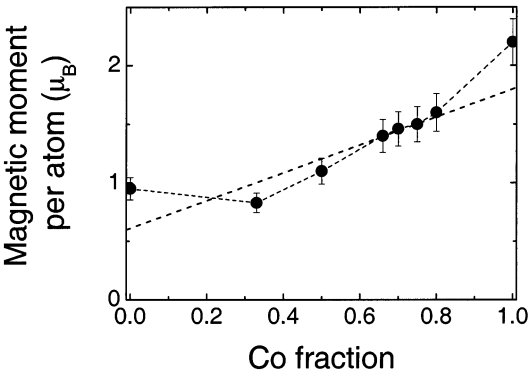

Figure 9. Magnetic moment per atom at 3 K for a 6-T applied magnetic field (filled circles) as a function of the Co fraction in the system obtained for the samples Co_xNi_{100-x}. For comparison, the dashed line represents the values for bulk Co−Ni alloys.

In fact, free Co^{2+} and Ni^{2+} ions have large magnetic moments (the spin-only magnetic moments are 3.87 μ_B and 2.82 μ_B, respectively). However the occurrence of a fraction of ions large enough to cause the observed magnetic moment increase would make the magnetization not saturate even at the highest applied field, whereas we observe saturation at field of ca. 2 T. Even the presence of cobalt or nickel oxides and silicates can be ruled out, in agreement with the TEM results. In fact, these compounds are antiferromagnetic at 4 K, which would make the total magnetic moment smaller than that expected if all of the nanoparticles were metallic.

Theoretical and experimental results indicate that 3d- and 4d-metal nanoclusters can present enhanced magnetic moments as a result of a reduction in the atomic coordination at their surfaces.[11,34−36] This effect has been observed both in Ni nanoparticles[11,34] smaller than (about 2 nm) or comparable to ours and in Co nanoparticles larger or much smaller[7,37,38] than ours. We

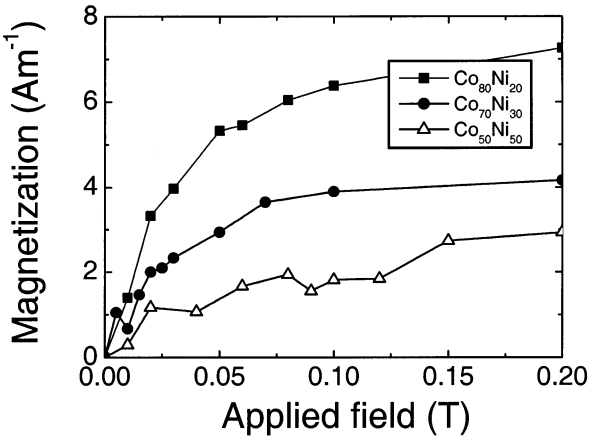

Figure 10. Demagnetization curve (represented in terms of the magnetic moment per film volume) at 300 K for the $Co_{50}Ni_{50}$, $Co_{70}Ni_{30}$, and $Co_{80}Ni_{20}$ samples.

observed an enhancement with respect to the bulk value around 30% for pure Co nanoparticles, whereas values reported in the literature so far are at most 20% even for particles much smaller than those synthesized in the present work. Because the magnetic moment generally increases with decreasing particle size,[34] we can conclude that the size is not the only parameter to be considered. On the other hand, in nanostructured materials (granular, epitaxial, and multilayered films), the chemical bonding between the surface of the nanostructure and the surrounding matrix plays a major role.[2,3] Even though the mechanism underlying the increase of the magnetic moment is still not clear, it is reasonable to assume that the modification at the surface caused by the interaction with the silica matrix is responsible for the observed behavior. The fact that we observed an increase that, within the experimental error, is among the highest ever reported can be ascribed to the particular sol−gel technique used.

What we found more surprising is that the same increase was not observed for the alloy-based nanocomposites. Electronic structures of alloys are different from those of metals because of the different crystal structures and, mainly, the chemical order. Co−Ni alloys are chemically very stable: this is one of the reasons these materials are largely used for magnetic recording media.[39] Probably, the chemical stability is conserved when these materials are reduced to nanosize, thus reducing the chemical interaction effects that lead to the magnetic moment enhancement.

The magnetic behavior at room temperature was studied by hysteresis measurements. Figure 10 shows the first quadrant of the demagnetization curves of the $Co_{80}Ni_{20}$, $Co_{70}Ni_{30}$, and $Co_{50}Ni_{50}$ samples. For all of the samples, neither hysteretic behavior nor remanent magnetization are observed. The absence of irreversible processes is characteristic of magnetic nanoparticles with superparamagnetic behavior.[3,4,40] This behavior appears when thermal demagnetization effects are so large that the magnetic moment can overcome the magnetic barriers that hinder the free inversion of the

(34) Apsel, S. E.; Emmert, J. W.; Deng, J.; Bloomfield, L. A. *Phys. Rev. Lett.* **1996**, *76* (9), 1441−1444.
(35) Cox, A. J.; Louderback, G.; Bloomfield, L. A. *Phys. Rev. Lett.* **1993**, *71*923−926.
(36) Vitos, L.; Johansson, B.; Kollar, J. *Phys. Rev. B: Condens. Matter* **2000**, *62* (18), R11957−R11960.
(37) Bucher, J. P.; Douglas, D. C.; Bloomfield, L. A. *Phys. Rev. Lett.* **1991**, *66* (23), 3052−3055.
(38) Hickey, B. J.; Howson, M. A.; Greig, D.; Wiser, N. *Phys. Rev. B*: *Condens. Matter* **1996**, *53* (1), 32−33.
(39) Li, X. G.; Murai, T.; Chiba; Takahashi, A. *J. Appl. Phys.* **1999**, *86* (4), 1999.
(40) El-Hilo, M.; O'Grady, K.; Chantrell, R. W. *J. Magn. Magn. Mater.* **1992**, *117*, 21−28.

magnetization. These barriers depend on the particle volume and the magnetic anisotropy of the material. In our case, either the small particle size or the reduced anisotropy barrier associated with the fcc structure of the Co−Ni nanoparticles[5] determines the occurrence of superparamagnetic behavior at room temperature. Studies are in progress to analyze the relationship between the superparamagnetic behavior and the morphological or structural features of these alloy-based nanoparticles.

4. Conclusion

In this work, the formation of Co−Ni alloy nanoparticles embedded in a silica host and synthesized with the sol−gel technique has been reported. The clusters exhibit an fcc structure for all of the compositions investigated, with a lattice parameter that is a growing function of the Co fraction in the samples. The excellent morphological and structural features (small particle size, narrow particle distribution, and small volumetric particle concentration) of the composites prepared by this sol−gel procedure are ideal for studying the influence of size in the alloy-based nanoparticles, and in the Co−Ni case, for analyzing the effects on the magnetic properties of stabilization of the fcc structural phase in Co-rich alloys. An enhancement of the magnetic moment was detected in the pure Co and Ni samples, and good agreement between the measured values and the values for the corresponding bulk alloys was found in the other cases. The different behaviors of the alloy-based nanoparticles and the metal-based nanoparticles can be related to the greater chemical stability of the alloy-based ones. At room temperature, an absence of remanence and coercivity is observed in the hysteresis loops, which is related to the superparamagnetic behavior of the fcc nanoparticles.

Acknowledgment. This work was partially supported by the MURST National University Research Project and by CNR National Project MSTA II.

CM021106R